Self-Assembled Core-Shell CdTe/poly(3-hexylthiophene) Nanoensembles as Novel Donor-Acceptor Light Harvesting Systems

Emin Istif,[a,†] Antonia Kagkoura,[b,†] Javier Hernandez-Ferrer,[a] Anastasios Stergiou,[b] Theodosis Skaltsas,[b] Raul Arenal,[c,d] Ana M. Benito,[a] Wolfgang K. Maser,[a*] and Nikos Tagmatarchis [b*]*

[a.] Instituto de Carboquimica ICB-CSIC, C/Miguel Luesma Castan 4, 50018 Zaragoza, Spain

[b.] Theoretical and Physical Chemistry Institute, National Hellenic Research Foundation, 48 Vassileos Constantinou Avenue, Athens 11635, Greece

[c.] Laboratorio de Microscopias Avanzadas, Instituto de Nanociencia de Aragon, Universidad de Zaragoza, 50018 Zaragoza, Spain

[d.] ARAID Foundation, 50018 Zaragoza, Spain

KEYWORDS: polymer nanoparticles • quantum dots • core-shell nanoparticles • donor-acceptor nanoensembles • energy conversion.

ABSTRACT: The self-assembly of novel core-shell nanoensembles consisting of regioregular poly(3-hexylthiophene) nanoparticles ($P3HT_{NPs}$) of 100 nm as core and semiconducting CdTe quantum dots ($CdTe_{QDs}$) as shell with a thickness of a few tens of nanometres was accomplished

by employing a re-precipitation approach. The structure, morphology and composition of $CdTe_{QDs}$/$P3HT_{NPs}$ nanoensembles were confirmed by high-resolution scanning transmission microscopy and dynamic light scattering studies. Intimate interface contact between the $CdTe_{QDs}$ shell and the $P3HT_{NPs}$ core leads to the stabilization of the $CdTe_{QDs}$/$P3HT_{NPs}$ nanoensemble as probed by steady-state absorption spectroscopy. Effective quenching of the characteristic photoluminescence of $CdTe_{QDs}$ at 555 nm, accompanied by simultaneous increase of emission of $P3HT_{NPs}$ at 660 and 720 nm, reveals photoinduced charge-transfer processes. Probing the redox properties of films of $CdTe_{QDs}$/$P3HT_{NPs}$ further proves the formation of a stabilized core-shell system in the solid-state. Photoelectrochemical assays on $CdTe_{QDs}$/$P3HT_{NPs}$ films show a reversible on-off photoresponse at a bias voltage of +0.8 V with a three times increased photocurrent compared to $CdTe_{QDs}$. The improved charge separation is directly related to the unique core-shell configuration, in which the outer $CdTe_{QDs}$ shell forces the $P3HT_{NPs}$ core to effectively act as electron acceptor. The creation of novel donor-acceptor core-shell hybrid materials via self-assembly is transferable to other types of conjugated polymers and semiconducting nanoparticles. This work, therefore, opens new pathways for the design of improved optoelectronic devices.

1. INTRODUCTION

The high demand for sustainable alternatives to fossil fuels brings solar energy conversion amongst the hottest research areas. In photosynthesis, solar energy is converted to chemical via multiple energy and electron transfer processes. Multi-component architectures, involving electron donor and acceptor moieties, are continuously developing to exploit this fundamental natural process and convert sunlight into electricity.[1, 2] Among the different electron donors, semiconducting quantum dots (QDs) are quite versatile materials and widespread employed.[3, 4] Markedly, QDs possess size-dependent physicochemical properties and particularly, the ability of tunable absorption and emission of light, as a function of their size and shape, after photoexcitation,[5] renders them ideal materials for managing energy conversion processes and participate in a variety of photoelectrochemical,[6-7] electronic and optoelectronic applications.[8-10] Within the semiconducting QDs based on the II-VI main groups element, $CdTe_{QDs}$ characterized by p-type behavior with 1.5 eV band-gap, is among the most extensively examined electron donor species, mainly due to the availability of numerous synthetic routes.[11, 12]

On the other hand, π-conjugated semiconducting polymers possessing relatively large absorption cross-section, owed to the delocalized π-electron transition from the ground to the singlet excited state, and high fluorescence efficiency, are viable candidates for the development of novel ensembles for managing charge-transfer processes. This, for example, has been shown in bulk heterojunction solar cells, where conjugated polymers and co-polymers were employed as electron donors blended with QDs as acceptors within the active layer,[13-17] covalently linked onto QDs surfaces[18, 19] and self-assembled with QDs.[20]

Especially, poly(3-hexylthiophene), abbreviated as P3HT, is a conjugated polymer with unique electronic properties and great potential for the development of optoelectronic devices. Notably,

while easily processable from solutions, the semi-crystalline character of P3HT favors high carrier mobility. Upon film formation, regioregular P3HT, abbreviated as rrP3HT, can self-assemble into 2D π-stacked lamellar structures, which can create carrier transport paths and improve charge mobility,[21] charge photogeneration and organic photovoltaic device power conversion efficiency.[22] Specifically, rrP3HT provides a head-to-tail arrangement allowing for the formation of a planar structure characterized by an effective charge transport and absorption range in the low energy part of the visible spectrum.[23]

In contrast to the planar assemblies of rrP3HT, in the past five years, photoactive semiconducting spherical nanoparticles with average diameter around 120 nm, arising from the solvent-induced aggregation of the π-conjugated chain of rrP3HT, have been developed.[24] For example, the generation of rrP3HT nanoparticles, abbreviated as $P3HT_{NPs}$ by the re-precipitation technique, contains rapid addition of the polymer solution in a selective solvent (e.g. tetrahydrofuran) to an excess volume of non-selective solvent (e.g. water). Both solvents must be miscible in order to collapse the polymer chain forming the nanoparticles.[25] During the addition of the polymer solution in tetrahydrofuran (THF) to water, the hydrophobic polymer hexyl chains disfavor the contact with the aqueous environment, thereby, fold to effectively adapt a stable spherical shape.[26] The $P3HT_{NPs}$ have attracted considerable attention owing to environmental friendly processing and their electron donating properties.[24] In this frame, $P3HT_{NPs}$ have been combined with other types of organic species or inorganic nanoparticles, furnishing novel donor-acceptor ensembles, in which upon photoexcitation charge-transfer processes prevail, en route to the design and development of optoelectronic devices. Hence, $P3HT_{NPs}$ have been functionalized with an indene C_{60} bisadduct (ICBA) forming water dispersible $P3HT_{NPs}$/ICBA ensembles, which upon fabrication in an organic photovoltaic device exhibited power conversion efficiency of up

to 2.5%.[27] Along the same lines, integrating phenyl-C_{61}-butyric acid methyl ester (PCBM) as an acceptor resulted to the fabrication of core-shell nanoparticles, where the emission of $P3HT_{NPs}$ was found quenched,[22, 28, 29] indicating the development of photoinduced electron-transfer phenomena from the nanoparticles to the fullerene derivative.[28] Photovoltaic devices based on mesoscale interconnected networks of nanoscale aggregates of such polymer nanoparticles revealed a comparable to typical bulk heterojunction devices performance,[29] while thin film active layer blends with inorganic electron acceptors, exhibited longer photoinduced electron transfer processes than organic acceptors.[15] Moreover, apart from the previously mentioned precipitation technique, $P3HT_{NPs}$:PCBM nanoparticles were also fabricated by a mini-emulsion method with the latter leading to greater amounts of crystalline P3HT domains as revealed by transient absorption spectroscopy.[22] Furthermore, decoration of $P3HT_{NPs}$ with Au nanoparticles led to the formation of nanostructured systems with photocatalytic activity towards the degradation of methylene blue with an efficiency up to 91%.[30]

The objective of the current work is three-fold, namely, to (i) prepare a $CdTe_{QDs}$ shell around a $P3HT_{NPs}$ core, (ii) identify electronic communication between the two species, upon visible photoillumination, and (iii) evaluate the generated photocurrent within the organic-inorganic ensembles. Herein, we study the electron accepting properties of $P3HT_{NPs}$ within core-shell $CdTe_{QDs}/P3HT_{NPs}$ ensembles and to the best of our knowledge this is the first time that a rrP3HT derivative functions as electron acceptor. Photoluminescence studies together with electrochemistry and photoelectrochemistry reveal strong intra-ensemble electronic communication under visible light irradiation, while transport of electrons from $CdTe_{QDs}$ to $P3HT_{NPs}$ within the $CdTe_{QDs}/P3HT_{NPs}$ ensembles yields an enhanced photocurrent generation in comparison to bare $CdTe_{QDs}$.

2. EXPERIMENTAL SECTION

2.1 General

Chemicals, reagents and solvents were purchased from Sigma Aldrich and used as received. Dry THF was distilled over benzophenone and sodium. Electronic absorption spectra (UV-Vis) were recorded on a Perkin–Elmer (Lambda 19) UV-Vis-NIR spectrophotometer. Dynamic light scattering (DLS) measurements were performed on a ALV/CGS-3 Compact Goniometer System (ALV GmbH, Germany), equipped with a JDS Uniphase 22mW He–Ne laser, operating at 632.8 nm, interfaced with an ALV-5000/EPP multi-tau digital correlator with 288 channels and an ALV/LSE-5003 light scattering electronics unit for a stepper motor drive and limiting switch control. The scattering intensity and correlation functions were measured at 90°. Correlation functions were collected for ten times and analyzed by the cumulant method and the CONTIN software, which provide the apparent hydrodynamic radii distributions by Laplace inversion of the correlation function and with the aid of the Stokes–Einstein relationship. Steady state emission spectra were recorded on a Fluorolog-3 Jobin Yvon-Spex spectrofluorometer (model GL3-21). Picosecond time-resolved fluorescence spectra were measured by the time-correlated single photon counting (TCSPC) method on a Nano-Log spectrofluorometer (Horiba Jobin Yvon), by using a laser diode as an excitation source (NanoLED, 482nm). Lifetimes were evaluated with the DAS6 Fluorescence-Decay Analysis Software. The experimental calculation of the quantum yield (Φ^{F}_{q}) for $CdTe_{QDs}$ and $P3HT_{NPs}$ in aqueous media was performed with Rhodamine B as reference fluorophore. Electrochemical studies were performed using a standard three-electrode cell. Glassy carbon was used as a working electrode, and platinum wires were used as counter and pseudoreference electrodes. Bu_4NPF_6 (98%) was recrystallized three times from acetone and dried in a vacuum at 100 °C before being used as an electrolyte. Before each

experiment, the cell was purged with Ar for 30 s. Glassy carbon, platinum mesh and saturated calomel electrode (SCE) were used as the working, counter and reference electrodes, respectively. Measurements were recorded using an EG&G Princeton Applied Research potentiostat/galvanostat 2273A connected to a personal computer running the PowerSuite software. The working electrode was cleaned before each experiment through polishing with a cloth and 6, 3, and 1 mm diamond pastes. The energy levels are calculated from the electrochemically determined onset redox potentials, which are converted into electronic energies[31, 32] by employing a conversion potential of 4.70 V (SHE potential of 4.44 V plus an additional potential of 0.26 V induced by the SCE reference). Photoelectrochemical measurements were carried out in a three-electrode cell fitted with a quartz window. Light from a 150 W Xe arc lamp (LOT-Oriel GmbH) illuminated the working electrodes. These consisted of films of $P3HT_{NPs}$, $CdTe_{QDs}$ and $P3HT_{NPs}/CdTe_{QDs}$, spray-coated on cleaned FTO electrodes from an appropriate volume (1 mL) of the corresponding water dispersion, covering a surface area of 1 cm x 1 cm. Data were recorded with an AUTOLAB PGSTAT302N potentiostat. Ag/AgCl electrode and Pt wire were used as reference and counter electrodes, respectively. The Supporting electrolyte consisted of a 0.1 M $NaClO_4$ solution in acetonitrile. Acetonitrile was dried out using a 3A molecular sieves and $NaClO_4$ was dehydrated in an oven at 150 °C overnight before use. The scan rate for cyclic voltammetry was 20 mV/s, and potentiostatic photocurrent transients were recorded at 0.8 V vs. Ag/AgCl. For the imaging analyses, the samples were prepared by dispersing $CdTe_{QDs}/P3HT_{NPs}$ in water, ultrasonicate and deposit a drop on a 3 mm copper grid supporting a very thin carbon membrane. High-resolution scanning transmission electron microscopy (HR-STEM) and energy-dispersive X-rays studies were performed on a probe-corrected STEM FEI Titan-Low-Base operating at 120 and 300 kV (fitted

with a X-FEG® gun and Cs-probe corrector (CESCOR from CEOS GmbH)). Molecular weight distributions of rrP3HT were determined by size exclusion chromatography (SEC) using a Waters system, composed of a Waters 1515 isocratic pump, a set of three μ-Styragel mixed bed columns (having a porosity range of 102 to 106 Å), a Waters 2414 refractive index detector (equilibrated at 40 °C) and controlled through Breeze software. THF was the mobile phase, used at a flow rate of 1.0 mL/min at 30 °C. The setup was calibrated with linear polystyrene standards having narrow polydispersity and weight average molecular weights in the range of 1200 to 929,000 g/mol. The samples were readily soluble in the mobile phase. Concentrations in the range 2-4 mg/mL were used for analysis. ^{1}H-NMR spectra of samples were recorded in $CDCl_3$ at 25 °C on a Bruker AV500 spectrometer at an operating frequency of 500.13 MHz.

2.2 Preparation of $CdTe_{QDs}$/$P3HT_{NPs}$ ensembles

Initially, rrP3HT in THF (1 mL, at a concentration of 1 mg/mL) was prepared and left stirring overnight at room temperature. Then, rrP3HT (1 mL) was injected into an aqueous solution of $CdTe_{QDs}$ (10 mL) under vigorous stirring. The dispersion was first stirred for 30 min at room temperature and then heated to 50 °C allowing the evaporation of THF to furnish $P3HT_{NPs}$/$CdTe_{QDs}$. The preparation of rrP3HT and $CdTe_{QDs}$ is described in detail in the Supporting Information, while spectroscopic characterization is provided in Figures S1 and S2.

3. RESULTS AND DISCUSSION

The preparation of $CdTe_{QDs}$/$P3HT_{NPs}$ nanoensembles was accomplished by an *in-situ* re-precipitation approach[25, 26] involving a THF solution of rrP3HT (1mL) and a water dispersion of $CdTe_{QDs}$ (10 mL). Essentially, the process involves three steps as illustrated in Scheme 1: (i) dissolving the polymer (P3HT) into a selective solvent (THF), (ii) mixing of the obtained solution with a marginal solvent (water), which has to be completely miscible with the selective solvent, and (iii) removal of the organic solvent by evaporation to leave behind water dispersible nanoparticles. During the second step, rapid diffusion of the selective solvent into the marginal

solvent occurs whereby the polymer chains in the selective solvent tend to avoid entering in contact with water. In order to achieve minimum exposure, they fold and assemble into spheroidal nanoparticles, before becoming into contact with the water phase. Taking advantage of this process, $CdTe_{QDs}$ can be deposited on the as-formed $P3HT_{NPs}$ and establish the $CdTe_{QDs}/P3HT_{NPs}$ assembly, in which $CdTe_{QDs}$ is the core and $P3HT_{NPs}$ is the shell. At this point it is important to emphasize that the dissolved P3HT chains and the $CdTe_{QDs}$ are present in the two different solvent phases (selective and marginal) and only can interact which each other once the $P3HT_{NPs}$ are rapidly formed in the selective phase upon injection into the aqueous $CdTe_{QDs}$ phase. Therefore, encapsulation of $CdTe_{QDs}$ within $P3HT_{NPs}$ in this kinetically driven process is unlikely. This is different to processes where materials are present in one solvent, which favors encapsulation as it is demonstrated for example by π-conjugated molecular systems (e.g. porphyrins).[33, 34]

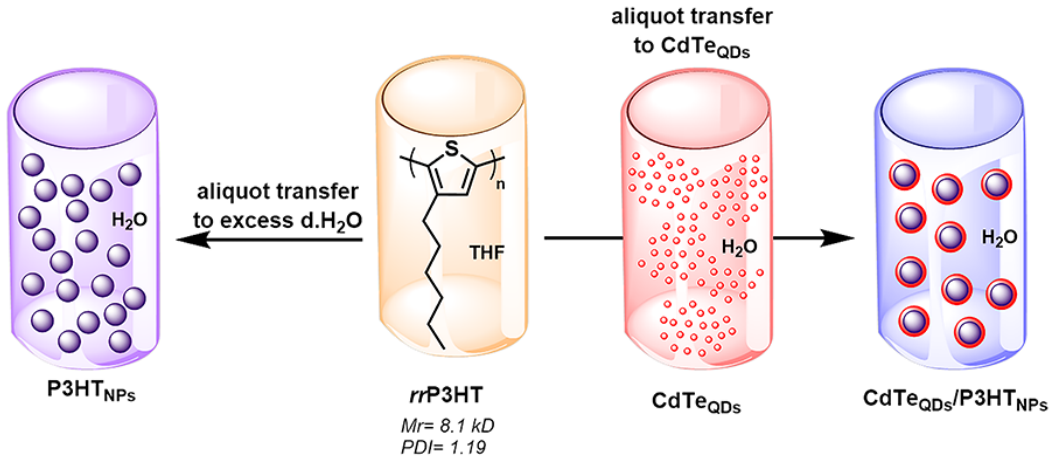

Scheme 1. Illustrative preparation of $CdTe_{QDs}/P3HT_{NPs}$ ensembles by following the re-precipitation technique, involving rapid injection of a rrP3HT solution in THF to an excess volume of distilled water under vigorous stirring.

Individual $CdTe_{QDs}/P3HT_{NPs}$ nanoensembles were imaged by scanning transmission electron microscopy (STEM) techniques. Figure 1 shows the presence of $CdTe_{QDs}/P3HT_{NPs}$ "bean-like" ensembles of around 150-250 nm in size. Hydrophilic $CdTe_{QDs}$, 2-7 nm in diameter, were found

attached onto the surface of the hydrophobic $P3HT_{NPs}$. The bare $P3HT_{NPs}$ and agglomerates of $CdTe_{QDs}$ reveal sizes in the range of 80 to 90 nm and 10 to 30 nm, respectively (Supporting Information, Figure S3). Evidently, the size of $P3HT_{NPs}$ is smaller than those of the $CdTe_{QDs}/P3HT_{NPs}$ ensembles. No changes in the structure/morphology and the composition of the bare $CdTe_{QDs}$ were observed (Supporting Information, Figure S3d, f) with respect to the ones in $CdTe_{QDs}/P3HT_{NPs}$ (Figure 1).

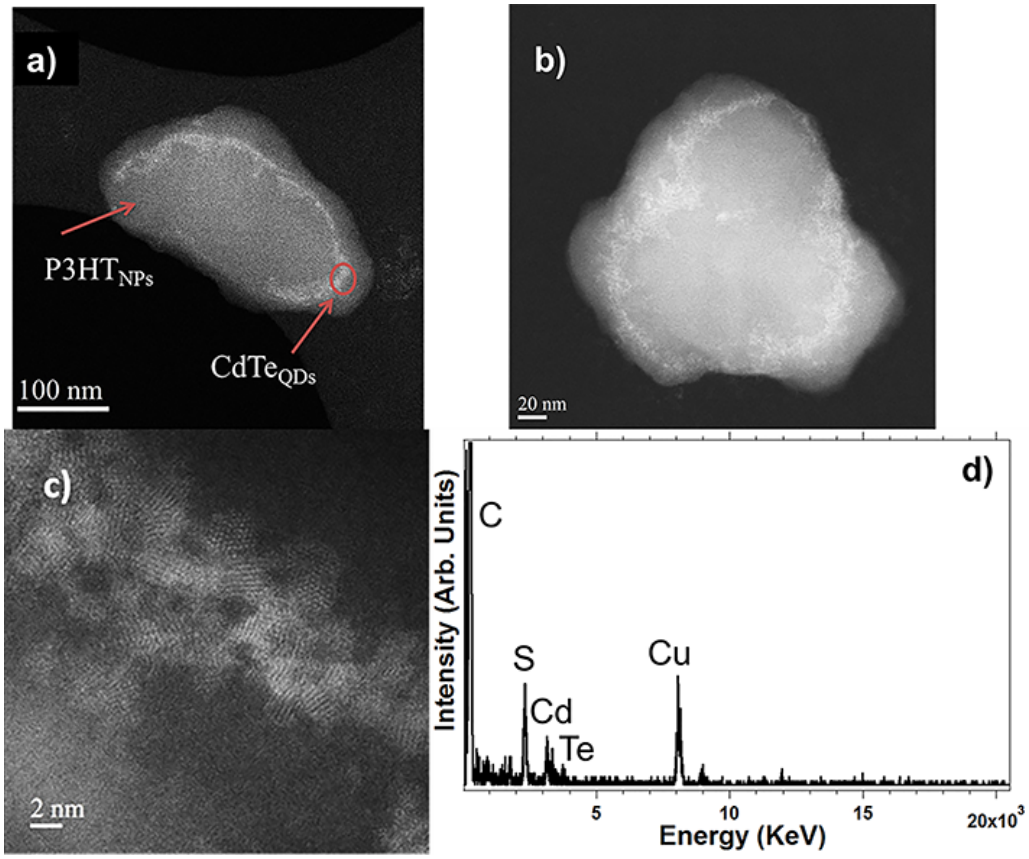

Figure 1. (a, b) High-angle annular dark-field (HAADF)-STEM images of two different $CdTe_{QDs}/P3HT_{NPs}$ ensembles at lower and higher magnification, respectively. (c) High-resolution HAADF-STEM micrograph showing the $CdTe_{QDs}$ located at the surface of $P3HT_{NPs}$. (d) EDS spectrum for $CdTe_{QDs}/P3HT_{NPs}$ ensembles. Scale bar is 50 nm.

In order to collect additional information regarding the size distribution of $CdTe_{QDs}$ and $P3HT_{NPs}$ as well as of the aqueous $CdTe_{QDs}/P3HT_{NPs}$ ensembles, dynamic light scattering (DLS) measurements on the corresponding systems in solution were performed. The average hydrodynamic radius (R_h) for the individual $P3HT_{NPs}$ and $CdTe_{QDs}$ was calculated to be 53 and 17 nm, respectively, while the R_h for the $CdTe_{QDs}/P3HT_{NPs}$ ensembles was found to be 110 nm (Supporting Information, Figure S4), which is in agreement with the sizes observed under STEM conditions (around 200 nm in diameter in average). In the case of individual $P3HT_{NPs}$, a small increase of their size was identified in DLS studies compared with STEM images, probably due to swelling of the polymer particles in liquid phase, whereas in $CdTe_{QDs}/P3HT_{NPs}$ ensembles this increase was not observed, most likely due to the $CdTe_{QDs}$ shell preventing the polymer particle swelling. On the other hand, $CdTe_{QDs}$ were found at ca. 34 nm in diameter, corresponding to $CdTe_{QDs}$ agglomerates, observed also with STEM (Supporting Information, Figure S3d), most possibly due to local aggregation phenomena arising from the inability of the small sized surface stabilizer (2-mercaptopropionic acid) of $CdTe_{QDs}$ to suppress the attraction across the interior bimetallic cores. Concluding, $P3HT_{NPs}$ tend to assemble in larger particles upon interaction with $CdTe_{QDs}$ forming $CdTe_{QDs}/P3HT_{NPs}$ ensembles due to interactions of $CdTe_{QDs}$ with the hydrophobic surface of the polymer particles. The high magnification STEM imaging of $CdTe_{QDs}/P3HT_{NPs}$ (Figure 1c) displays the $CdTe_{QDs}$ shell around $P3HT_{NPs}$ with an average thickness of 6-30 nm. This observation further clarifies the size difference between bare $P3HT_{NPs}$ (around 85 nm) and $CdTe_{QDs}/P3HT_{NPs}$ (around 200 nm) in the solid state and is also related with the DLS findings, where the presence of trapped water molecules within the polymer chain and the $CdTe_{QDs}$ is also associated to the expansion of the $CdTe_{QDs}/P3HT_{NPs}$ particles (R_h around 110 nm) as compared to bare $P3HT_{NPs}$ (R_h around 50 nm). Independent of subtle size differences

related to the technique and the probed system, both STEM and DLS studies confirm the formation of $CdTe_{QDs}/P3HT_{NPs}$ core-shell ensembles, consisting of a $P3HT_{NPs}$ core of about 100 nm in diameter and a shell formed by $CdTe_{QDs}$ with a layer thickness of a few tens of nanometres. Collectively, DLS along with TEM data are summarized in Table 1.

Table 1. Diameter of the materials as calculated by DLS measurements and observed by TEM imaging.

Material	R_h/Diameter[a] (nm)	Diameter by TEM[b] (nm)
$P3HT_{NPs}$	53/106	80-90
$CdTe_{QDs}$	17/34	10-30[c] (2-7)
$CdTe_{QDs}/P3HT_{NPs}$	110/220	150-250

[a] Apparent hydrodynamic radii as calculated by the cumulant analysis method from DLS measurements (see experimental).

[b] Approximate diameter as observed from TEM images.

[c] The size corresponds to $CdTe_{QDs}$ aggregates, in parenthesis is the size of the single quantum dots.

Steady-state electronic absorption spectroscopy was employed to track the formation of $CdTe_{QDs}/P3HT_{NPs}$ ensembles by monitoring the characteristic absorptions of $P3HT_{NPs}$. The rrP3HT in THF exhibits a strong, broad and featureless π-π* transition around 445 nm due to its conjugated polymer backbone (Figure 2 (a)). Upon formation of $P3HT_{NPs}$, the π-π* transition considerably red-shifts to 505 nm. Being still broad, its low energy zone additionally is characterized by a rich vibronic band structure. These observations clearly indicate the change of the morphology of the rrP3HT chains into $P3HT_{NPs}$.[24] The vibronic peaks appear at 505, 550 and 600 nm and are assigned as the A_{0-2}, A_{0-1} and A_{0-0} peaks, respectively. These are attributed to crystalline P3HT aggregates within the $P3HT_{NPs}$. By contrast, the featureless high energy

shoulder represents the non-aggregated, i.e. amorphous domains within the $P3HT_{NPs}$.[24] On the other hand, the absorption spectrum of $CdTe_{QDs}$ is characterized by a typical shoulder centred at 520 nm. In the case of the $CdTe_{QDs}/P3HT_{NPs}$ ensembles, the absorption of $P3HT_{NPs}$ was further red-shifted by about 10 nm. This latter indicates electronic communication between $CdTe_{QDs}$ (or aggregates thereof) and $P3HT_{NPs}$ at the core-shell interface. Moreover, the enhancement of the intensity of the A_{0-0} vibrational peak with respect to the A_{0-1} peak suggest an interaction of the $CdTe_{QDs}$ with the amorphous domains $P3HT_{NPs}$, located at the core-shell interface (please note that the A_{0-0} transition is forbidden, albeit it becomes allowed due to the presence of amorphous domains and interacting species).[35]

Next, focusing on identifying possible electronic interplay at the excited states of $CdTe_{QDs}/P3HT_{NPs}$, photoluminescence assays were performed. Results for the core-shell system and its constituents are shown in Figure 2 (b). The emission spectrum of pristine $CdTe_{QDs}$ upon excitation at 490 nm was governed by a broad band centred at 555 nm, while the emission spectrum of $P3HT_{NPs}$ upon excitation at 490 nm exhibits a wide emission band at 640-750 nm, showing two peaks at 660 and 720 nm, which can be associated to the 0-0 and 0-1 emissions of $P3HT_{NPs}$.[36, 37] Notably, in the $CdTe_{QDs}/P3HT_{NPs}$ ensembles the characteristic emission of $CdTe_{QDs}$ was quenched by 65%, for samples possessing identical concentrations, while at the same time the emission due to $P3HT_{NPs}$ was significantly increased. The suppression of the photoluminescence is attributed to effective immobilization of $CdTe_{QDs}$ onto $P3HT_{NPs}$, calling also for the development of strong electronic interactions at the excited state between the two species within $CdTe_{QDs}/P3HT_{NPs}$. The latter quenching of the band owed to $CdTe_{QDs}$, centred at 555 nm, is due to charge-transfer as the decay mechanism of the singlet excited state of $CdTe_{QDs}$. In order to shed light on the photoluminescence quenching mechanism and the dynamics of the

system, time-resolved photoluminescence lifetime assays were performed. Time-correlated-single-photon-counting measurements were employed to acquire the fluorescence lifetime profiles for $CdTe_{QDs}$/$P3HT_{NPs}$. The fluorescence decay profile of bare $CdTe_{QDs}$ was measured and correlated with the one owed to $CdTe_{QDs}$/$P3HT_{NPs}$. Exciting $CdTe_{QDs}$ at 482 nm, the emission at 555 nm was best monoexponentially fitted. It should be noted that although biexponential fitting was employed for the bare $CdTe_{QDs}$, the analysis of the quenching mechanism was based focusing on the dominant population for convenience. Analysis of the function revealed the fluorescence emission lifetime for pristine $CdTe_{QDs}$ to be 29 ns (Supporting Information, Figure S5). However, the measurable decay component in $CdTe_{QDs}$/$P3HT_{NPs}$, corresponding to the quenching of the photoluminescence intensity in the steady-state spectra, was not identified, implicitly suggesting that the excited state deactivation of $CdTe_{QDs}$ in $CdTe_{QDs}$/$P3HT_{NPs}$ is faster than the 50 ps resolution of our instrumentation. Then, upon excitation at 482 nm, focusing on the emission of $P3HT_{NPs}$ at 720 nm, within the $CdTe_{QDs}$/$P3HT_{NPs}$ ensemble, the photoluminescence decay was monoexponentially fitted and analyzed to be 0.43 ns. The latter value, higher than the one calculated for the bare $P3HT_{NPs}$ (ca. 0.35 ns), is attributed to the excited state of $P3HT_{NPs}$ within $CdTe_{QDs}$/$P3HT_{NPs}$. Overall, these results are in full accordance with the steady-state measurements, showing that the photoluminescence suppression of $CdTe_{QDs}$ is accompanied by a simultaneous enhancement of the emission owed to $P3HT_{NPs}$ (Figure 2 (b)) for the $CdTe_{QDs}$/$P3HT_{NPs}$ ensembles. Considering the fast decay value of 50 ps as the upper limit of the actual lifetime attributed to the excited state of $CdTe_{QDs}$ in $CdTe_{QDs}$/$P3HT_{NPs}$, consistent with the strong emission quenching of $CdTe_{QDs}$ by $P3HT_{NPs}$ as identified in the steady-state photoluminescence measurements, and comparing the lifetime values for $CdTe_{QDs}$/$P3HT_{NPs}$ with those for the individual species $CdTe_{QDs}$ and $P3HT_{NPs}$, the minimum value for the quenching rate

constant (k^S_q) for the excited state of $CdTe_{QDs}$ and the quenching quantum yield (Φ^S_q) in $CdTe_{QDs}/P3HT_{NPs}$ were calculated according to equations 1 and 2 to be $1.995x10^8$ s^{-1} and 0.998, respectively.

Equation 1: $k^S_q = (1/\tau_f)-(1/\tau_o)$

Equation 2: $\Phi^S_q = [(1/\tau_f)-(1/\tau_o)]/(1/\tau_f)$

τ_f refers to the lifetime of $CdTe_{QDs}$ in $CdTe_{QDs}/P3HT_{NPs}$ and τ_o refers to the lifetime of bare $CdTe_{QDs}$.

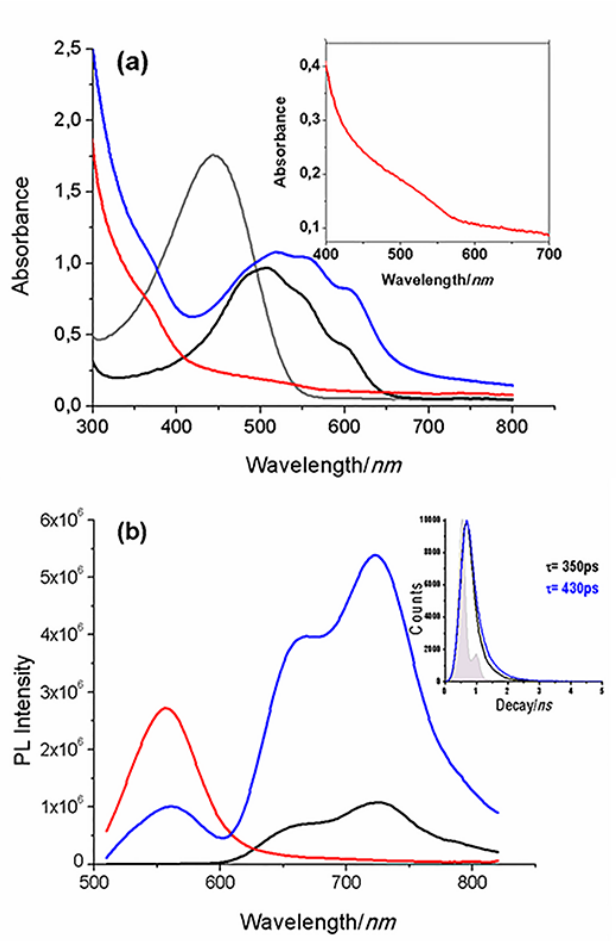

Figure 2. (a) UV-Vis absorption spectra for rrP3HT (grey), obtained in THF, and $P3HT_{NPs}$ (black), $CdTe_{QDs}$ (red) and $CdTe_{QDs}/P3HT_{NPs}$ (blue), obtained in H_2O. Inset: Expanded area of the

absorption spectrum of $CdTe_{QDs}$. (b) Photoluminescence spectra for $P3HT_{NPs}$ (black), $CdTe_{QDs}$ (red) and $CdTe_{QDs}/P3HT_{NPs}$ (blue), obtained upon excitation at 490 nm in H_2O. Inset: Fluorescence lifetime decay profiles for $P3HT_{NPs}$ (black) and $CdTe_{QDs}/P3HT_{NPs}$ (blue).

Next, focusing on the electrochemical properties and the conduction and valence band energy levels of the materials, cyclic voltammetry (CV) studies were performed (Figure 3). The CV curve for $P3HT_{NPs}$ showed two reversible oxidations and one reversible reduction, likewise the ones identified for rrP3HT, however, with diminutive changes in the oxidation/reduction onset potentials. The onset potential for the first oxidation peak of $P3HT_{NPs}$ found to be at +0.50 V, while the onset potential for the reduction peak evolves at -1.80 V. These values result in an electrochemical gap of 2.30 eV, which is slightly narrower than the corresponding one of rrP3HT registered at 2.42 eV. The first oxidation and reduction onset potentials for rrP3HT found as high as +0.52 and -1.90 V, respectively. The lower electrochemical gap for $P3HT_{NPs}$ is a consequence of an enhanced degree of crystalline aggregation, in agreement with the UV-Vis results (Figure 2 (a)). Indeed, the first oxidation peak is indicative for crystalline aggregates, while the second one represents the amorphous phases.[38] For $P3HT_{NPs}$, the first oxidation peak associated to the crystalline aggregations is strongly increased ca. by a factor of 2 with respect to the amorphous parts. The increased crystallinity of $P3HT_{NPS}$ equally well is observed at the reduction site. The CV studies on $P3HT_{NPs}$ thus show a response typical for a semicrystalline P3HT with a high degree of crystalline domains.[39] On the other hand, the CV curve for $CdTe_{QDs}$ reveals two irreversible oxidation steps and one irreversible reduction process, at +0.36 and +0.95, and -1.00 V, respectively, with a narrow electrochemical gap of 1.36 eV, in agreement with similar reports in the literature.[40, 41] Finally, in the CV curve for the $CdTe_{QDs}/P3HT_{NPs}$ ensembles, two broad irreversible oxidation peaks and a quasi-reversible reduction process appear. The broad shape of

the oxidation peaks is characteristic of the $CdTe_{QDs}$ redox properties and the onset potential at +0.45 V for $CdTe_{QDs}/P3HT_{NPs}$ is associated with the oxidation of $CdTe_{QDs}$, masking the oxidation of $P3HT_{NPs}$. On the other side, the reduction response reveals a different behavior and supports the formation of a novel $CdTe_{QDs}/P3HT_{NPs}$ system. The appearance of a quasi-reversible reduction peak at -1.60 V, proper to the new $CdTe_{QDs}/P3HT_{NPs}$ system underlines an easier reduction process by 200 mV as compared to the bare $P3HT_{NPs}$ and thus highlights the enhanced stabilization of the core-shell system as also observed in the UV-Vis studies (Figure 2 (a)). Table 2 summarizes the data for the photophysical and electrochemical properties of rrP3HT, $P3HT_{NPs}$, $CdTe_{QDs}$ and $CdTe_{QDs}/P3HT_{NPs}$ ensembles.

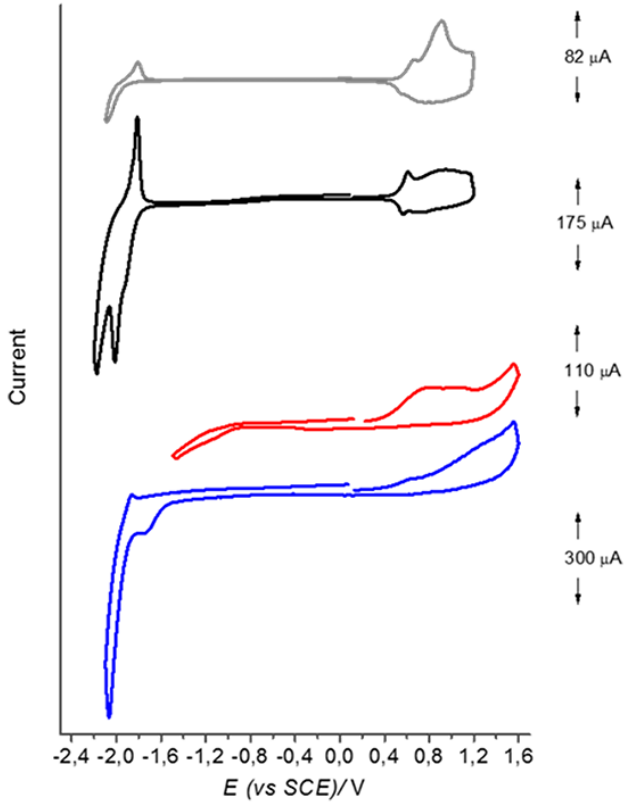

Figure 3. Cyclic voltammetry graphs for rrP3HT (grey), $P3HT_{NPs}$ (black), $CdTe_{QDs}$ (red), and $CdTe_{QDs}/P3HT_{NPs}$ ensembles (blue), recorded in acetonitrile under nitrogen-saturated atmosphere and in the presence of 0.1M Bu_4NPF_6 as electrolyte.

Table 2. Summarized data for the photophysical and electrochemical properties of rrP3HT, $P3HT_{NPs}$, $CdTe_{QDs}$ and $CdTe_{QDs}/P3HT_{NPs}$ ensembles. Potential values are expressed vs the SCE reference electrode at 25 °C. The data of the fluorescence emission and the related lifetimes (τ_f) were recorded after excitation at 490 nm and 482 nm, respectively.

Materials	**Electrochemical properties**		**Photophysical properties**					
	Redox Potentials/V	**E_g[a]/eV**	**Abs/nm**	**Emi/nm**	**τ_f/ns**	**k^S_q(s^{-1})**	**Φ^S_q**	**Φ^F_q[b]**
rrP3HT	+0.52, +0.64, -1.90	2.42	445	573	0.53[c]	-	-	-
$P3HT_{NPs}$	+0.50, +0.65, -1.80, -1.85	2.35	480, 505, 550, 605	660, 720	0.35	-	-	0.07
$CdTe_{QDs}$	+0.36, +0.95, -1.00	1.36	525	555	29[c]	-	-	0.25
$P3HT_{NPs}/CdTe_{QDs}$	+0.45, +0.86, -1.60, -1.83	2.05	485, 515, 555, 610	555, 660, 720	0.43	$1.995x10^8$	0.998	-

[a] Calculated from the CV data.

[b] Fluorescence quantum yields are experimentally calculated, in aqueous media, with Rhodamine B (Φ^F_q = 0.49 in ethanol) as reference.

[c] Decay profiles are shown in the Supporting Information, Figure S5.

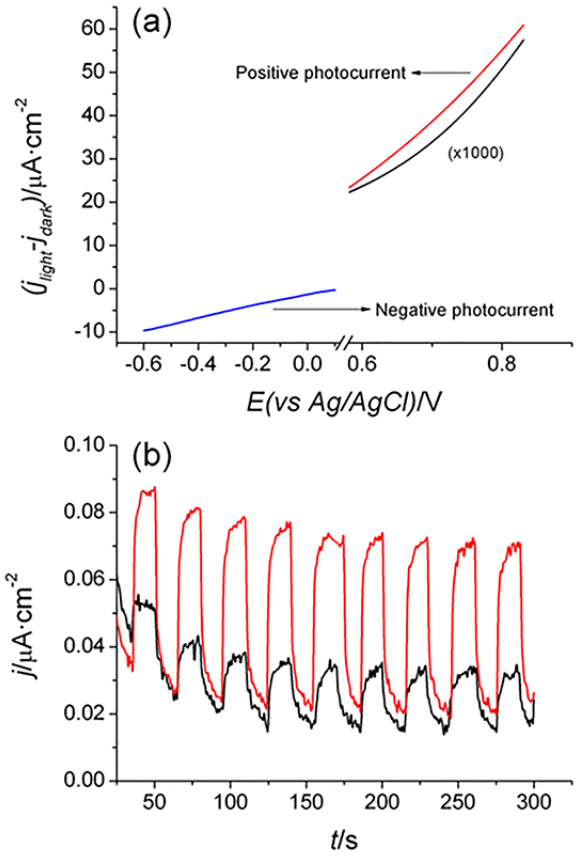

Figure 4. (a) Difference of current densities under illumination and dark conditions obtained from the cyclic voltammograms of films of $P3HT_{NPs}$ films (blue), $CdTe_{QDs}$ (black) and $CdTe_{QDs}/P3HT_{NPs}$ (red). (b) Photocurrent generation response of films of $CdTe_{QDs}$ (black) and $CdTe_{QDs}/P3HT_{NPs}$ (red) at an applied voltage of 0.8 V vs Ag/AgCl reference electrode under illumination.

Finally, photoelectrochemical measurements were performed in a three-electrode cell fitted with a quartz window, in 0.1 M $NaClO_4$ as the redox electrolyte in acetonitrile, employing a Ag/AgCl reference electrode and a Pt wire as counter electrode. Briefly, the working electrode consisting of either $P3HT_{NPs}$, $CdTe_{QDs}$ or $CdTe_{QDs}/P3HT_{NPs}$ films fabricated by spray-coating on FTO substrates covering an area of 1 cm x 1 cm was illuminated with white light and the observed

photocurrent was measured. Figure 4 (a) shows the differences of the current densities under illumination and dark conditions as obtained from the cyclic voltammograms (I-V characteristics). The $P3HT_{NPs}$/FTO electrode reveals a negative photocurrent in the range from 0 V to -0.6 V, where it decreases from 0 to -10 $\mu A/cm^2$, indicative for improved charge separation under applied bias voltage. Positive photocurrents were not observed. This photoanodic response is typical for n-type semiconductors and proves that $P3HT_{NPs}$ accepts electrons. On the contrary, $CdTe_{QDs}$/FTO and $CdTe_{QDs}$/$P3HT_{NPs}$/FTO electrodes show a distinct behavior. They exhibit a positive photocurrent in the range from 0 V to 0.8 V. Negative photocurrents were not observed. This photocathodic response is typical for p-type semiconductors and points out that $CdTe_{QDs}$ donates electrons.

Being also the case for the $CdTe_{QDs}$/$P3HT_{NPs}$ film, it is suggested that the interface to the electrolyte is formed by only $CdTe_{QDs}$. The latter is in direct agreement with the STEM observations, which show that $CdTe_{QDs}$ are tightly deposited on the $P3HT_{NPs}$ forming a shell covering the $P3HT_{NPs}$ core in the $CdTe_{QDs}$/$P3HT_{NPs}$ ensemble. Moreover, the maximum enhancement of the photocurrent, achieved at a bias voltage around 0.8 V, reaches about 50 nA/cm^2. This is ca. 20 % higher with respect to the bare for the $CdTe_{QDs}$/FTO electrode. Hence, electron injection from the reduced $P3HT_{NPs}$, as generated by charge-separation via the singlet excited state of $CdTe_{QDs}$, to the FTO electrode occurs, proving that $P3HT_{NPs}$ act as an acceptor. More insight on the enhancement of the photocurrent is provided by transient photocurrent response measurements.

Figure 4 (b) shows the transient photocurrent response of $CdTe_{QDs}$ and $CdTe_{QDs}$/$P3HT_{NPs}$ films under illumination, measured at an applied potential of 0.8 V over several cycles. The photocurrent responses were prompt, steady, and reproducible during repeated on/off cycles of

the light illumination. Eliminating short time capacitive currents, the photocurrent for the $CdTe_{QDs}$/$P3HT_{NPs}$/FTO electrode reaches values, which are almost 3 times higher as compared to the ones of the $CdTe_{QDs}$/FTO electrode. This result is also in agreement with the I-V characteristics (*cf*. Figure 4 (a)), thus highlighting the superiority of $CdTe_{QDs}$/$P3HT_{NPs}$/FTO over $CdTe_{QDs}$/FTO. The improved charge transfer/separation in the $CdTe_{QDs}$/$P3HT_{NPs}$ system is a direct consequence of the unique self-assembly possibilities of rrP3HT in the presence of aqueous dispersions and to form a core-shell system. Figure 5 shows the energy levels of the conduction and the valence band for the individual $CdTe_{QDs}$ and the $P3HT_{NPs}$ as well as those for the $CdTe_{QDs}$/$P3HT_{NPs}$ nanoassembly, respectively, as calculated from redox data (cf. Figure 3 and Table 2). As for the individual materials concerns, the conduction band of $CdTe_{QDs}$ resides at lower energy as compared to that of $P3HT_{NPs}$, hence making energetically unfavourable the electron flow from the former to the latter component (Figure 5a). However, the picture reverses when it comes to $P3HT_{NPs}$/$CdTe_{QDs}$, namely, the energy level of the conduction band owed to $CdTe_{QDs}$ is increased, thereby allowing diffused photoexcited electrons to travel towards the conduction band of $P3HT_{NPs}$ within the nanoensemble (Figure 5b).[42] Even though the real energy levels at the core-shell interface forming a p-n junction cannot be precisely calculated, since redox processes take place at the material-electrode interface, the big picture is a type II alignment of the energy bands within the $CdTe_{QDs}$/$P3HT_{NPs}$ ensemble. This type of supramolecular arrangement is highly versatile and can be easily extended to other types of conjugated polymers and inorganic semiconducting nanoparticles in order to obtain novel nanometre-sized core-shell particles with tuneable photophysical properties of interest for improved optoelectronic devices.

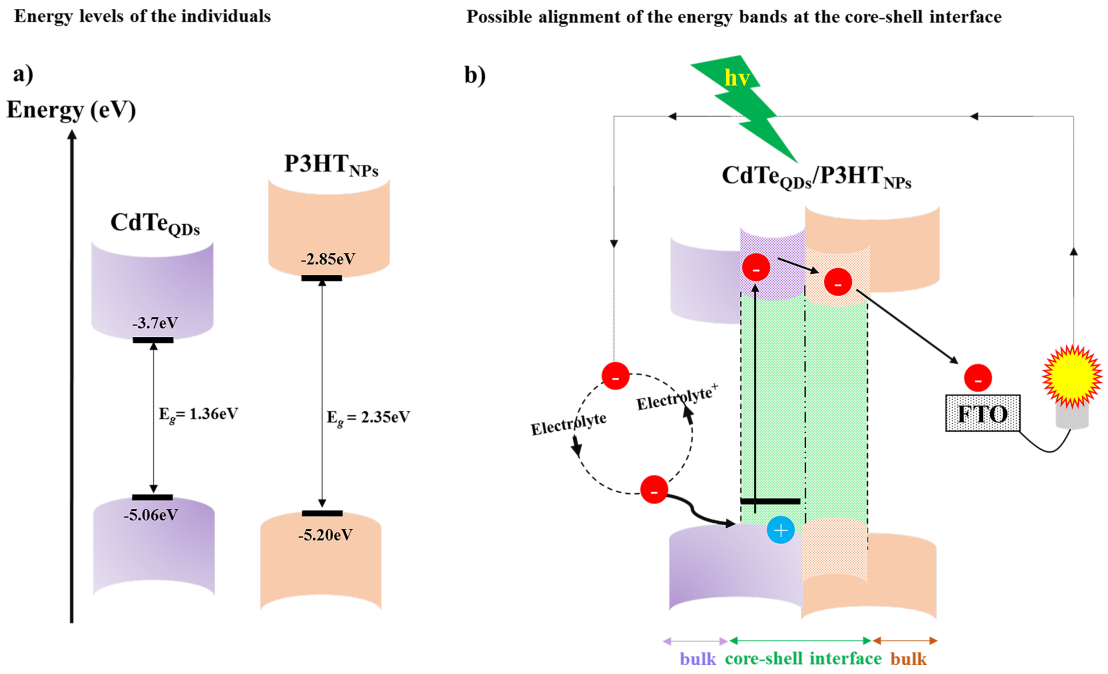

Figure 5. Energy diagram for (a) individual $CdTe_{QDs}$ and $P3HT_{NPs}$ as calculated from CV assays, and (b) $CdTe_{QDs}/P3HT_{NPs}$ ensembles at the core-shell interface forming a p-n junction.

4. CONCLUSION

Using a re-precipitation approach involving the rapid injection of a rrP3HT THF solution into an aqueous dispersion of semiconducting $CdTe_{QDs}$ quantum dots, the self-assembly of novel core-shell nanoparticle ensembles was achieved for the first time. The core of the $CdTe_{QDs}/P3HT_{NPs}$ ensemble consists of semicrystalline $rrP3HT_{NPs}$ nanoparticles of about 100 nm in diameter while the shell is formed by agglomerated $CdTe_{QDs}$ quantum dots exhibiting a layer thickness of a few tens of nanometers. The $CdTe_{QDs}/P3HT_{NPs}$ core-shell ensembles are characterized by an intimate interaction between the outer amorphous part of the $P3HT_{NPs}$ core and the $CdTe_{QDs}$ shell. This leads to the stabilization of the $CdTe_{QDs}/P3HT_{NPs}$ core-shell system as revealed by a lower P3HT π-π^* transition. Moreover, it yields in the effective quenching of the photoluminescence of the

shell forming $CdTe_{QDs}$ and thus confirms the existence of charge transfer processes at the interface between the $CdTe_{QDs}$ shell and the $P3HT_{NP}$ core forming an effective donor-acceptor system, respectively. The electrochemical response on films further supports the findings of a stabilized $CdTe_{QDs}/P3HT_{NPs}$ core-shell system in the solid state. Furthermore, at a bias voltage of +0.8 V, $CdTe_{QDs}/P3HT_{NPs}$ films show a prompt, steady and reproducible on-off photoresponse consisting of a three times enhanced photocurrent with respect to $CdTe_{QDs}$. The possibility to synthesize novel organic-inorganic core shell ensembles with tunable donor-acceptor behavior and superior photophysical properties via simple self-assembly processes employing conjugated polymers and inorganic semiconducting nanoparticles may open new pathways for the design of improved optoelectronic devices.

SUPPORTING INFORMATION

The Supporting Information is available free of charge on the ACS Publications website. Experimental section including synthesis of 2,5-dibromo-3-hexylthiophene, synthesis of regioregular poly(3-hexylthiophene) (rrP3HT), preparation of $CdTe_{QDs}$, ^{1}H-NMR spectrum, SEC curve, high-angle annular dark-field-STEM and bright-field-STEM images and EDS-STEM spectrum.

AUTHOR INFORMATION

Corresponding Author

*Emails: wmaser@icb.csic.es (W. K. Maser); abenito@icb.csic.es (A. M. Benito); tagmatar@eie.gr (N. Tagmatarchis)

Author Contributions

[†]These authors have equally contributed to this work.

ACKOWLEDGEMENTS

This work has received funding from the European Union's Horizon 2020 research and innovation programme under the Marie Sklodowska-Curie grant agreement No 642742. AMB and WKM gratefully acknowledge financial support from Spanish MINECO under project ENE206-79282-C5-1-R and its associated European Regional Development Fund, as well as the Government of Aragon under project DGA-T66 and associated European Social Fund. RA gratefully acknowledges financial support from Spanish MINECO under project MAT2016-79776-P and its associated European Regional Development Fund, as well as the Government of Aragon under project DGA-E26 and associated European Social Fund. The STEM studies were conducted at the Laboratorio de Microscopias Avanzadas, Instituto de Nanociencia de Aragon, Universidad de Zaragoza, Spain. The authors would like to thank Esteban Urriolabeitía for carrying out the NMR studies.

REFERENCES

1. Barber, J. Photosynthetic Energy Conversion: Natural and Artificial. *Chem. Soc. Rev.* **2009**, *38*, 185-196.

2. Nocera, D. G. The Artificial Leaf. *Acc. Chem. Res.* **2012**, *45*, 767–776.

3. Resch-Genger, U.; Grabolle, M., Cavaliere-Jaricot, S.; Nitschke, R.; Nann, T. Quantum Dots Versus Organic Dyes as Fluorescent Labels. *Nat. Methods* **2008**, *5*, 763-775.

4. Kundu, S.; Patra, A. Nanoscale Strategies for Light Harvesting. *Chem. Rev.* **2017**, *117*, 712-757.

5. Santra P. K.; Kamat, P.V. Tandem-Layered Quantum Dot Solar Cells: Tuning the Photovoltaic Response with Luminescent Ternary Cadmium Chalcogenides. *J. Am. Chem. Soc.* **2013**, *135*, 877-885.

6. Han, Q.; Wang, R.; Xing, B.; Zhang, T.; Khan, M. S.; Wu, D. ; Wei, Q. Label-free Photoelectrochemical Immunoassay for CEA Detection Based on CdS Sensitized WO_3@BiOI Heterostructure Nanocomposite. *Biosens. Bioelectron.***2018**, *99*, 493-499.

7. Li, X.; Wang, Y.; Shi, L.; Ma, H.; Zhang, Y.; Du, B.; Wu, D.; Wei, Q. A Novel ECL Biosensor for the Detection of Concanavalin A Based on Glucose Functionalized $NiCo_2S_4$ Nanoparticles-grown on Carboxylic Graphene as Quenching Probe. *Biosens. Bioelectron.* **2017**, *96*, 113-120.

8. Michalet, X.; Pinaud, F. F.; Bentolila, L. A.; Tsay, J. M.; Doose, S.; Li, J. J.; Sundaresan, G.; Wu, A. M.; Gambhir, S. S.; Weiss, S. Quantum Dots for Live Cells, in Vivo Imaging, and Diagnostics. *Science* **2005**, *307*, 538-544.

9. Talapin, D. V.; Lee, J.-S.; Kovalenko, M. V.; Shevchenko, E. V. Prospects of Colloidal Nanocrystals for Electronic and Optoelectronic Applications. *Chem. Rev.* **2010**, *110*, 389–458.

10. Meng, K.; Chen, G.; Thampi, K. R. Metal Chalcogenides as Counter Electrode Materials in Quantum Dot Sensitized Solar Cells: A Perspective. *J. Mater. Chem. A* **2015**, *3*, 23074-23089.

11. Kershaw, S. V.; Susha, A. S.; Rogach, A. L. Narrow Bandgap Colloidal Metal Chalcogenide Quantum Dots: Synthetic Methods, Heterostructures, Assemblies, Electronic and Infrared Optical Properties. *Chem. Soc. Rev.* **2013**, *42*, 3033-3087.

12. Zhuang, Z.; Peng, Q.; Li, Y. Controlled Synthesis of Semiconductor Nanostructures in the Liquid Phase. *Chem. Soc. Rev.* **2011**, *40*, 5492-5513.

13. Yao, S.; Chen, Z.; Li, F.; Xu, B.; Song, J.; Yan, L.; Jin, G.; Wen, S.; Wang, C.; Yang, B.; Tian, W. High-Efficiency Aqueous-Solution-Processed Hybrid Solar Cells Based on P3HT Dots and CdTe Nanocrystals. ACS *Appl. Mater. Interfaces* **2015**, *7*, 7146–7152.

14. Ren, S.; Chang, L.; Lim, S.; Zhao, J.; Smith, M.; Zhao, N.; Bulović, V.; Bawendi, M.; Gradečak, S. Inorganic–Organic Hybrid Solar Cell: Bridging Quantum Dots to Conjugated Polymer Nanowires. *Nano Lett.* **2011**, *11*, 3998–4002.

15. Noone, K. M.; Subramaniyan, S.; Zhang, Q.; Cao, G.; Jenekhe, S. A.; Ginger, D. S. Photoinduced Charge Transfer and Polaron Dynamics in Polymer and Hybrid Photovoltaic Thin Films: Organic vs Inorganic Acceptors. *J. Phys. Chem. C* **2011**, *115*, 24403–24410.

16. Yin, J.; Kumar, M.; Lei, Q.; Ma, L.; Raavi, K. S. S.; Gurzadyan, G.G.; Soci, C. Small-Size Effects on Electron Transfer in P3HT/InP Quantum Dots. *J. Phys. Chem. C* **2015**, *119*, 26783–26792.

17. Radychev, N.; Locteva, I.; Witt, F.; Kolny-Olesiak, J.; Borchert, H.; Parisi, J. Physical Origin of the Impact of Different Nanocrystal Surface Modifications on the

Performance of CdSe/P3HT Hybrid Solar Cells. *J. Phys. Chem. C* **2011**, *115*, 14111-14122.

18. Shi, Y.; Tan, L.; Chen, L.; Chen, Y. In Situ Fabricating One-Dimensional Donor–Acceptor Core–Shell Hybrid Nanobeams Network Driven by Self-Assembly of Diblock Copolythiophenes. *Macromolecules* **2014,** 47, 1757-1767.

19. Xu, J.; Wang, J.; Mitchell, M.; Mukherjee, P.; Jeffries-EL, M.; Petrich, W. J.; Lin, Z. Organic-Inorganic Nanocomposites via Directly Grafting Conjugated Polymers onto Quantum Dots. *J. Am. Chem. Soc.* **2007**, 129, 12828-12833.

20. Kim, J. Y.; Cho, H. C.; Paek, K.; Jo, M.; Park, M.; Lee, N.: Kim, Y.; Kim, J. B.; Lee, E. Precise Control of Quantum Dot Location within the P3HT-b-P2VP/ QD Nanowires Formed by Crystallization-Driven 1D Growth of Hybrid Dimeric Seeds. *J. Am. Chem. Soc.* **2014**, *136*, 2767–2774.

21. Han, Y.; Guo, Y.; Chang, Y.; Geng, Y.; Su, Z. Chain Folding in Poly(3-hexylthiophene) Crystals. *Macromolecules* **2014**, *47*, 3708-3712.

22. Schwarz, K. N.; Farley, S. B.; Smith, T. A.; Ghiggino, K. P. Charge Generation and Morphology in P3HT:PCBM Nanoparticles Prepared by Mini-Emulsion and Reprecipitation Methods. *Nanoscale* **2015**, *7*, 19899-19904.

23. Tremel, K.; Ludwigs, S. in *P3HT Revisited – From Molecular Scale to Solar Cell Devices*; Ludwigs, S., Ed.; Springer Berlin Heidelberg, Berlin, Germany, 2014; Chapter 2, pp 39-82.

24. Nagarjuna, G.; Baghgar, M.; Labastide, J. A.; Algaier, D. D.; Barnes, M. D.; Venkataraman, D. Tuning Aggregation of Poly (3-hexylthiophene) Within Nanoparticles. *ACS Nano* **2012**, *6*, 10750-10758.

25. Pecher, J.; Mecking, S. Nanoparticles of Conjugated Polymers. *Chem. Rev.* **2010**, *110*, 6260-6279.

26. Tuncel, D.; Demir, H. V. Conjugated Polymer Nanoparticles. *Nanoscale* **2010**, *2*, 484-494.

27. Ulum, S.; Holmes, N.; Barr, M.; Kilcoyne, A. L. D.; Gong, B. B.; Zhou, X.; Belcher, W.; Dastoor, P. The role of Miscibility in Polymer:Fullerene Nanoparticulate Organic Photovoltaic Devices. *Nano Energy* **2013**, *2*, 897-905.

28. Chambon, S.; Schatz, C.; Sébire, V.; Pavageau, B.; Wantz, G.; Hirsch, L. Organic Semiconductor Core-Shell Nanoparticles Designed Through Successive Solvent Displacements. *Mater. Horiz.* **2014**, *1*, 431-438.

29. Gehan, T. S.; Bag, M.; Renna, L. A.; Shen, X.; Algaier, D. D.; Lahti, P. M.; Russell, T. P.; Venkataraman, Multiscale Active Layer Morphologies for Organic Photovoltaics Through Self-Assembly of Nanospheres. D. *Nano Lett.* 2014, **14**, 5238-5243.

30. Jana, B.; Bhattacharyya, S.; Patra, A. Conjugated Polymer P3HT–Au Hybrid Nanostructures for Enhancing Photocatalytic Activity. *Phys. Chem. Chem. Phys.* **2015**, *17*, 15392-15399.

31. Trassati, S. The Absolute Electrode Potential: An Explanatory Note. *Pure Appl. Chem.* **1986**, *58*, 955-966.

32. Cardona, C.; Li, W.; Kaifer, A. E.; Stockdale. D.; Bazan, G. Electrochemical Considerations for Determining Absolute Frontier Orbital Energy Levels of Conjugated Polymers for Solar Cell Applications. *Adv. Mater.* **2011**, *23*, 2367–2371.

33. Hasobe, T.; Sandanayaka, A. S. D.; Wada, T.; Araki, Y. Fullerene-Encapsulated Porphyrin Hexagonal Nanorods. An Anisotropic Donor-Acceptor Composite for Efficient Photoinduced Electron Transfer and Light Energy Conversion. *Chem. Commun.* **2008**, *29*, 3372-3374.

34. Sandanayaka, A. S. D.; Murakami, T.; Hasobe, T. Preparation and Photophysical and Photoelectrochemical Properties of Supramolecular Porphyrin Nanorods Structurally Controlled by Encapsulated Fullerene Derivatives. *J. Phys. Chem. C* **2009**, *113*, 18369-18378.

35. Kohn, P.; Rong, Z.; Scherer, K. H.; Sepe, A.; Sommer, M.; Müller-Buschbaum, P.; Friend, R. H.; Steiner, U.; Hüttner, S. Crystallization-Induced 10-nm Structure Formation in P3HT/PCBM Blends. *Macromolecules* **2013** *46*, 4002-4013.

36. Baghgar, M.; Barnes, M. D. Work Function Modification in P3HT H/J Aggregate Nanostructures Revealed by Kelvin Probe Force Microscopy and Photoluminescence Imaging. *ACS Nano* **2015**, *9*, 7105-7112.

37. Niles, E. T.; Roehling, J. D.; Yamagata, H., Wise, A. J.; Spano, F. C. ; Moulé, A. J.; Grey, J. K. J-Aggregate Behavior in Poly-3-hexylthiophene Nanofibers. *J. Phys. Chem. Lett.* **2012**, *3*, 259-263.

38. Sweetnam, S.; Graham, K. R.; Ngongang Ndjawa, G. O.; Heumüller, T.; Bartelt, J. A.; Burke, T. M.; Li, W.; You, W.; Amassian, A.; McGehee, M. D. Characterization of the Polymer Energy Landscape in Polymer:Fullerene Bulk Heterojunctions with Pure and Mixed Phases. *J. Am. Chem. Soc.* **2014**, *136*, 14078-14088.

39. Egbe, D. A. M.; Nguyen, L. H.; Carbonnier, B.; Mühlbacher, D.; Sariciftci, N. S. Thiophene-Containing Poly(arylene–ethynylene)-*alt*-poly(arylene–vinylene)s: Synthesis, Characterisation and Optical Properties. *Polymer* **2005**, *46*, 9585-9595.

40. Amelia, M.; Lincheneau, C.; Silvi, S.; Credi, A. Electrochemical Properties of CdSe and CdTe Quantum Dots. *Chem. Soc. Rev.* **2012**, *41*, 5728-5743.

41. Poznyak, S. K.; Osipovich, N. P.; Shavel, A.; Talapin, D. V.; Gao, M.; Eychmüller, A. Gaponik, N. Size-Dependent Electrochemical Behavior of Thiol-Capped CdTe Nanocrystals in Aqueous Solution. *J. Phys. Chem. B* **2005**, *109*, 1094-1100.

42. Zhao, W.; Liu, Z.; Shan, S.; Zhang, W.; Wang J.; Ma, Z.; Xu, J.; Chen, H. Bismuthoxyiodide Nanoflakes/Titania Nanotubes Arrayed p-n Heterojunction and Its Application for Photoelectrochemical Bioanalysis. *Sci. Rep.* **2014**, *4*, 4426.

Supporting Information

Self-assembled core-shell CdTe/poly(3-hexylthiophene) nanoensembles as novel donor-acceptor light harvesting systems

Emin Istif,[a,†] Antonia Kagkoura,[b,†] Javier Hernandez-Ferrer,[a] Anastasios Stergiou,[b] Theodosis Skaltsas,[b] Raul Arenal,[c,d] Ana M. Benito,[a] Wolfgang K. Maser,[a*] and Nikos Tagmatarchis [b*]*

[a]Instituto de Carboquimica ICB-CSIC, C/Miguel Luesma Castan 4, 50018 Zaragoza, Spain.

[b]Theoretical and Physical Chemistry Institute, National Hellenic Research Foundation, 48 Vassileos Constantinou Avenue, Athens 11635, Greece.

[c]Laboratorio de Microscopias Avanzadas, Instituto de Nanociencia de Aragon, Universidad de Zaragoza, 50018 Zaragoza, Spain.

[d]ARAID Foundation, 50018 Zaragoza, Spain.

* Emails: wmaser@icb.csic.es (W. K. Maser); abenito@icb.csic.es (A. M. Benito); tagmatar@eie.gr (N. Tagmatarchis)

[†]These authors have equally contributed to this work.

EXPERIMENTAL SECTION

Synthesis of 2,5-dibromo-3-hexylthiophene

1.5 g (9 mmol) 3-hexylthiophene was dissolved in 25 mL dry DMF in round bottom flask and placed in ice bath. 3.2 g (18 mmol) N-bromosuccinimide (NBS) was dissolved in 10 mL dry DMF in another vial and added portion-wise on round bottom flask for 15 min under inert atmosphere. The reaction flask was covered with aluminum paper to protect it from light. After 1 h the ice bath was removed and the reaction was stirred overnight at room temperature. For purification, the reaction mixture was poured onto cold water and extracted with diethylether (3x50 mL). The separated organic phases were washed with brine and water, dried over Na_2SO_4 and filtered. Then, the solvent and remaining 3-hexylthiophene were removed under high vacuum at 90 °C, to yield 2,5-dibromo-3-hexyl thiophene (80%).

Synthesis of regioregular poly(3-hexylthiophene) (rrP3HT)

Regioregular P3HT was synthesized via a Grignard method according to literature.[1] In a flame dried Schlenk flask, 2,5-dibromo-3-hexyl thiophene (1g, 3 mmol) was dissolved in freshly dried THF (6 mL) and tert-BuMgCl (2.9 mL, 2.9 mmol, 1M in THF) was added with a syringe under inert atmosphere. The reaction mixture was stirred at room temperature for 3h. Subsequently, [1,3-bis(diphenylphosphino)propane]-dichloro nickel(II) ($Ni(dppp)Cl_2$) (64 mg, 0.12 mmol) was added to initiate the polymerization and the reaction mixture was stirred for 30 min at room temperature. The polymerization reaction was stopped by adding aqueous 5N HCl (2 mL). After precipitation in methanol the polymer was filtered into a Soxhlet thimble and extracted with methanol overnight to remove any unreacted monomer and low molecular weight impurities. The pure rrP3HT was obtained by dissolving the polymer in chloroform, followed by precipitation in methanol to yield 300 mg of rrP3HT. Regioregularity: 92%, MW: 8100 and PDI: 1.19 (see ESI, Figure S1 and S2).

Preparation of $CdTe_{QDs}$

The $CdTe_{QDs}$ were synthesized in aqueous phase by following a two-step procedure.[2, 3] Initially, NaHTe was prepared by dissolving Te (26 mg, 0.204 mmol) and $NaBH_4$ (100 mg, 2.64 mmol) in

distilled water (5 mL) with the aid of bath sonication for 30 minutes. After that period, the solution turned pink and was de-aerated by bubbling with nitrogen for 20 minutes. Subsequently, $Cd(ClO_4)_2$ (650 mg, 2.087 mmol) along with 2-mercaptopropionic acid (0.37 mL, 4 mmol) were dissolved in distilled water (125 mL) under stirring. Then the pH of the solution was adjusted to around 12 by adding dropwise aqueous 1M NaOH, followed by de-aeration by bubbling with nitrogen for 20 minutes. Afterwards, NaHTe was injected to the above solution with a syringe under stirring and nitrogen atmosphere and the reaction mixture was refluxed at 96 °C for 15 minutes and after that period the reaction mixture was exposed to air while continuing the reflux for 24 hours.

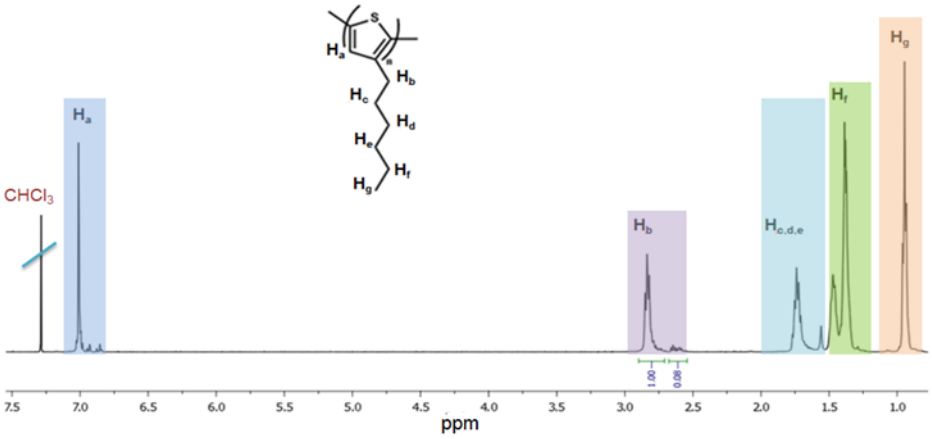

Figure S1. ^{1}H-NMR spectrum of rrP3HT obtained in $CDCl_3$.

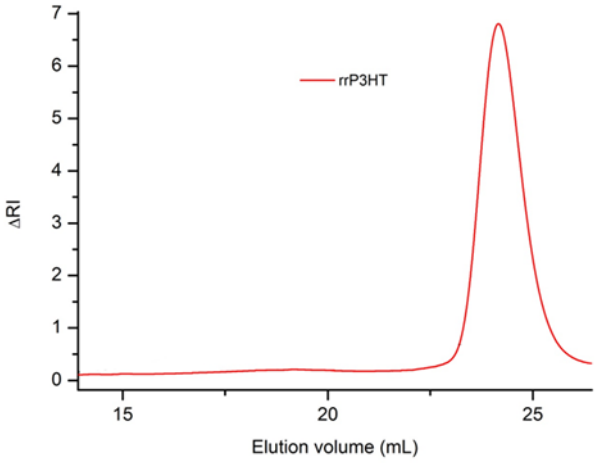

	Mw	PDI
rrP3HT	8.100	1,19

Figure S2. SEC curve for rrP3HT.

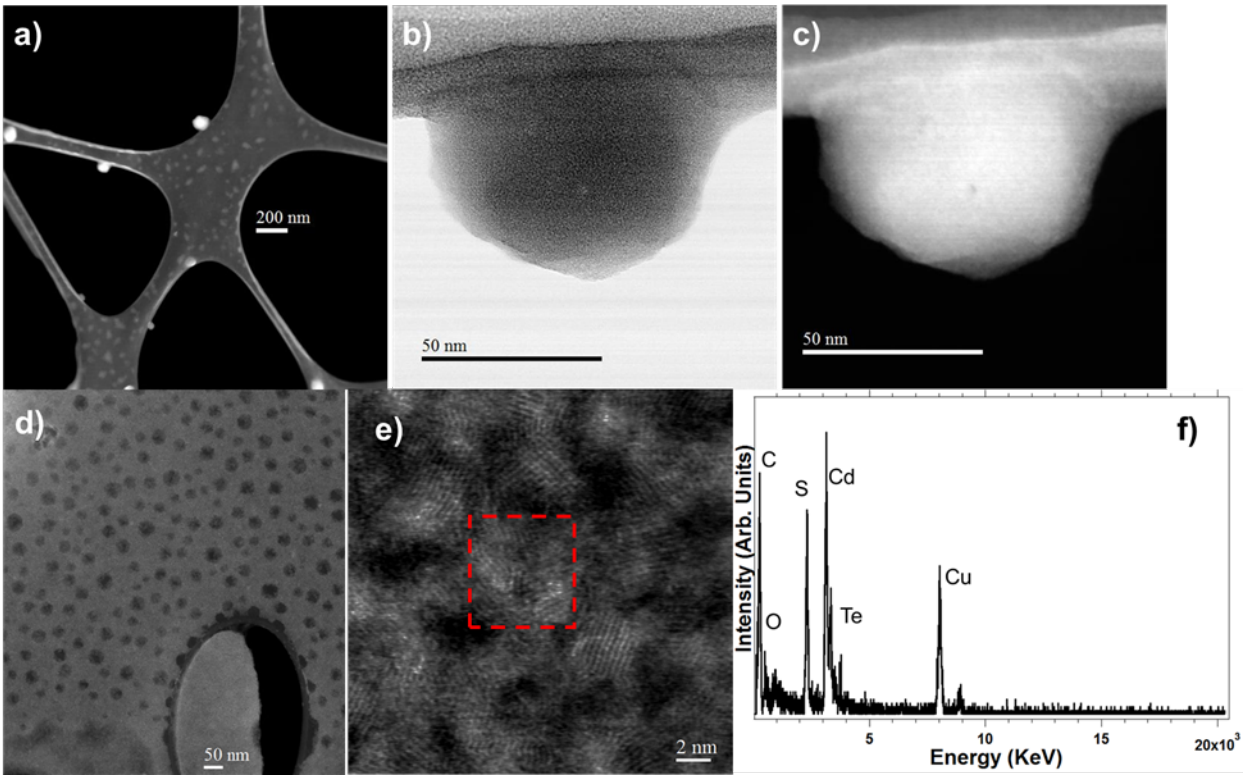

Figure S3. (a) and (c) High-angle annular dark-field (HADDF)-STEM images of $P3HT_{NPs}$ at lower and higher magnification, respectively. (b) Bright-field (BF)-STEM image of the same $P3HT_{NPs}$ displayed in (c). (d) BF-STEM image of several $CdTe_{QDs}$. (e) High-resolution HAADF-STEM micrograph showing $CdTe_{QDs}$. (f) EDS-STEM spectrum recorded by scanning the electron beam during 20 sec in the red rectangular area highlighted in the HAADF-STEM image shown in (e).

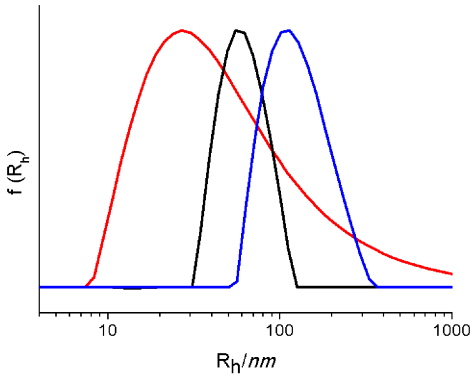

Figure S4. Size distribution graphs for $CdTe_{QDs}$(red), $P3HT_{NPs}$ (black) and $CdTe_{QDs}/P3HT_{NPs}$ (blue).

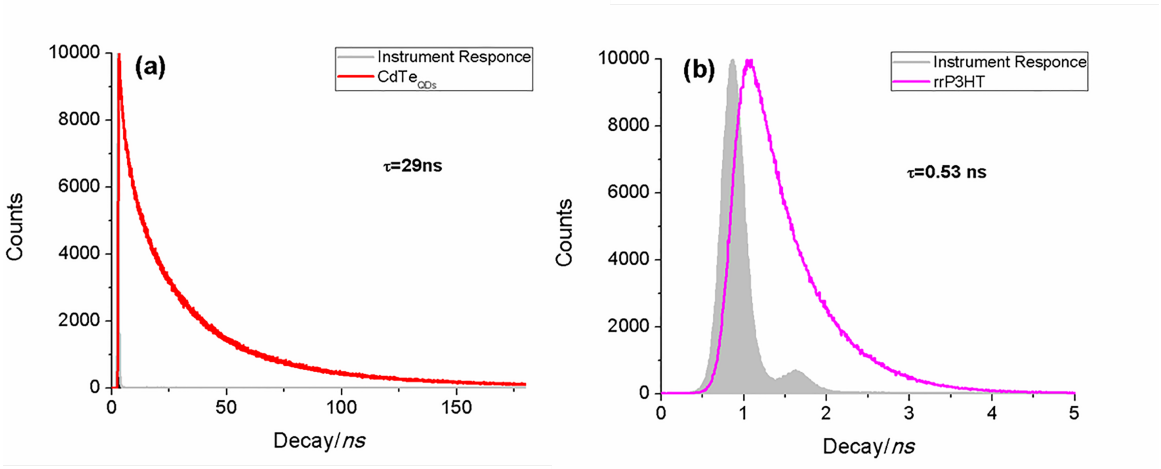

Figure S5. Fluorescence lifetime decay profiles for (a) $CdTe_{QDs}$ (excitation 482 nm, emission 555 nm), and (b) rrP3HT (excitation 482 nm, emission 720 nm)

REFERENCES

(1) Lohwasser, R. H.; Thelakkat, M. Toward perfect control of end groups and polydispersity in poly (3-hexylthiophene) via catalyst transfer polymerization. *Macromolecules*, **2011**, *44*, 3388-3397.

(2) Zhang, Y.; Li, Y.; Yan, X. P. Aqueous Layer-by-Layer Epitaxy of Type-II CdTe/CdSe Quantum Dots with Near-Infrared Fluorescence for Bioimaging Applications *Small*, **2009**, *5*, 185-189.

(3) Wang, J.; Han, H. Hydrothermal synthesis of high-quality type-II CdTe/CdSe quantum dots with near-infrared fluorescence. *J. Colloid Interface Sci*., **2010**, *351*, 83-87.